 CMES, vol.101, no.3, pp.207-228, 2014

Dynamic Response of Borehole in Poroelastic Medium with Disturbed Zone

W. Kaewjuea[1], T. Senjuntichai[2] and R.K.N.D. Rajapakse[3]

Abstract: Dynamic response of an infinite cylindrical borehole in a poroelastic medium with an excavation disturbed zone is investigated in this paper. The borehole is subjected to axisymmetric time-harmonic loads and fluid sources applied to its surface, which is either fully permeable or impermeable. The governing equations based on Biot's poroelastodynamics theory are solved by using two scalar potentials and two vector potentials. The general solutions are then derived through the application of Fourier integral transform with respect to the vertical coordinate. An exact stiffness matrix scheme is established from the derived general solutions to include the excavation disturbed zone. Boundary value problems corresponding to a borehole with the disturbed zone subjected to axisymmetric loads and fluid sources are formulated, and selected numerical results are presented to portray dynamic response of a borehole in a poroelastic medium with consideration of excavation disturbed zone.

Keywords: Borehole, Dynamic response, Exact stiffness matrix method, Excavation disturbed zone, Poroelasticity.

1 Introduction

The study of dynamic response of a cylindrical borehole in soils and rocks has useful applications to several engineering disciplines. For example, the analysis of impact, from gas explosion inside a mine, on the surrounding rock is important in evaluating the damage caused by gas explosions. In the past, several researchers [e.g. Jordan (1962); Parnes (1986)] investigated dynamic response of deep cylindrical borehole in an isotropic or transversely isotropic elastic medium to axisymmetric loading applied to the borehole surface. Geomaterials are generally two-phase materials with solid skeleton and pores filled with water, and commonly

[1] PSU, Songkhla, Thailand.
[2] CU, Bangkok, Thailand.
[3] SFU, Burnaby, BC, CA.

known as poroelastic materials. The first theory of elastic wave propagation in a poroelastic medium was established by Biot (1956) by adding inertia terms to his quasistatic theory [Biot (1941)]. A review of literature reveals that Biot's theory of poroelasticity [Biot (1941)] has been widely employed for investigating various problems related to quasi-static response of a cylindrical borehole in a poroelastic medium [Detornay and Cheng (1988); Rajapakse (1993); Cui, Cheng and Abousleiman (1997); Abousleiman and Chen (2010); Kaewjuea and Senjuntichai (2014)]. However, a limited number of studies related to dynamic response of a borehole in a poroelastic medium have appeared in the literature when compared to its quasi-static counterpart despite their relevance to geotechnical engineering and earthquake engineering. An example is a study by Lu and Jeng (2006), who considered a wave propagation problem related to an infinite borehole in a poroelastic medium.

Borehole drilling process is a primary factor in causing changes of physical, mechanical and hydraulic properties around the borehole such as bulk modulus, shear modulus, desaturation and strength [Sato, Kikuchi and Sugihara (2000)]. The soil or rock zone, where its properties are changed, is called an excavation disturbed zone (EDZ). The level of change depends on the soil/rock properties, the stress field, the borehole geometry, the drilling method and the excavation time. The EDZ is thus one of the most important factors that affect the stability of borehole and could have a significant influence on stresses and pore pressure in the vicinity of borehole. The characterization of the EDZ has been investigated over the last fifteen years by several researchers. For example, Sato, Kikuchi and Sugihara (2000) performed an excavation disturbed experiment at Tono mine in central Japan to observe the soil/rock properties change such as fracturing, stress redistribution and desaturation; and width of the EDZ induced by excavation process. The study of the character and the extent of excavation damage at the underground research laboratory (URL) located in Manitoba, Canada was presented by Martino and Chandler (2004). Later, Armand, Lebon, Cruchaudet, Rebours, Morel and Wileveau (2007), and Shao, Schuster, Sonnke and Brauer (2008) studied the geological and hydraulic characterization, the influence of rock mechanical properties and excavation method of EDZ at the URL Meuse/Haute-Marne in France. Kwon et al. (2008, 2009) investigated the influence of the EDZ on thermal, hydraulic and mechanical behaviors near the borehole during the construction of the KAERI underground research tunnel in Korea. It has been recommended that the EDZ should be considered as an important parameter during the design of underground facilities. A recent study by Kaewjuea and Senjuntichai (2014), who investigated quasi-static response of a cylindrical borehole in a poroelastic medium with disturbed zone, also confirms a significant influence from the EDZ on stresses and pore pressure in

the vicinity of borehole. To our knowledge, studies related to a cylindrical borehole in a poroelastic medium under dynamic loading with the consideration of excavation disturbed zone have never been reported in the literature.

This paper presents dynamic response of an infinite cylindrical borehole in a poroelastic medium with excavation disturbed zone subjected to axisymmetric time-harmonic loading. The general solutions are derived based on Biot's poroelastodynamics theory and Fourier transform. Both shear modulus and permeability of the medium are assumed to be changed from their original values in the disturbed zone. In the present study, the EDZ is discretized into a number of infinitely long tubular layers with small thickness and homogeneous properties perfectly bonded together. Boundary value problems corresponding to a borehole subjected to axisymmetric loading applied at its surface are formulated. Two extreme hydraulic boundary conditions at the borehole surface, i.e. fully permeable and impermeable surfaces, are considered. Selected numerical results are presented to portray the influence of poroelastic effects and the excavation disturbed zone on dynamic response of borehole.

2 Governing equations and general solutions

Consider an infinite cylindrical borehole in a poroelastic medium with excavation disturbed zone subjected to axisymmetric loadings defined with a cylindrical coordinate system (r,θ,z) as shown in Fig. 1. The governing equations for axisymmetric motions of a poroelastic medium, in the absence of body forces (solid and fluid) and a fluid source, can be expressed according to Biot (1962) as

$$\mu\nabla^2 u_r+(\lambda+\alpha^2M+\mu)\frac{\partial\varepsilon}{\partial r}-\mu\frac{u_r}{r^2}-\alpha M\frac{\partial\zeta}{\partial r}=\rho\ddot{u}_r+\rho_f\ddot{w}_r \tag{1}$$

$$\mu\nabla^2 u_z+(\lambda+\alpha^2M+\mu)\frac{\partial\varepsilon}{\partial z}-\alpha M\frac{\partial\zeta}{\partial z}=\rho\ddot{u}_z+\rho_f\ddot{w}_z \tag{2}$$

$$\alpha M\frac{\partial\varepsilon}{\partial r}-M\frac{\partial\zeta}{\partial r}=\rho_f\ddot{u}_r+m\ddot{w}_r+b\dot{w}_r \tag{3}$$

$$\alpha M\frac{\partial\varepsilon}{\partial z}-M\frac{\partial\zeta}{\partial z}=\rho_f\ddot{u}_z+m\ddot{w}_z+b\dot{w}_z \tag{4}$$

where $\nabla^2=\frac{\partial^2}{\partial r^2}+\frac{1}{r}\frac{\partial}{\partial r}+\frac{\partial^2}{\partial z^2}$; the superscript dot denotes the derivative of field variables with respect to the time parameter t; u_i and w_i denote the displacement in the i direction $(i=r,z)$ of the solid matrix and the fluid displacement relative to the solid displacement respectively; ε is the dilatation of the solid matrix; ζ is the variation of the fluid content per unit reference volume defined as $\zeta=-w_{i,i}$; μ and λ are the shear modulus and Lame′ constant of the bulk material respectively; ρ and ρ_f

denote the mass densities of the bulk material and the pore fluid respectively; m is a density-like parameter defined as $m = \rho_f/\beta$, in which β is porosity; and b is a parameter accounting for the internal friction due to the relative motion between the solid matrix and the pore fluid. If internal friction is neglected then b = 0. In addition, the parameters α ($0 \leq \alpha \leq 1$) and M ($0 \leq M < \infty$) are Biot's parameters accounting for compressibility of the two-phase material [Biot (1941)]. For a completely dry material, α=0 and M=0, whereas for a material with incompressible constituents, α= 1 and $M \to \infty$.

The constitutive relations for a homogeneous poroelastic material [Biot (1941)] can be expressed as

$$\sigma_{rr} = 2\mu \frac{\partial u_r}{\partial r} + \lambda \varepsilon - \alpha p \tag{5}$$

$$\sigma_{\theta\theta} = 2\mu \frac{u_r}{r} + \lambda \varepsilon - \alpha p \tag{6}$$

$$\sigma_{zz} = 2\mu \frac{\partial u_z}{\partial z} + \lambda \varepsilon - \alpha p \tag{7}$$

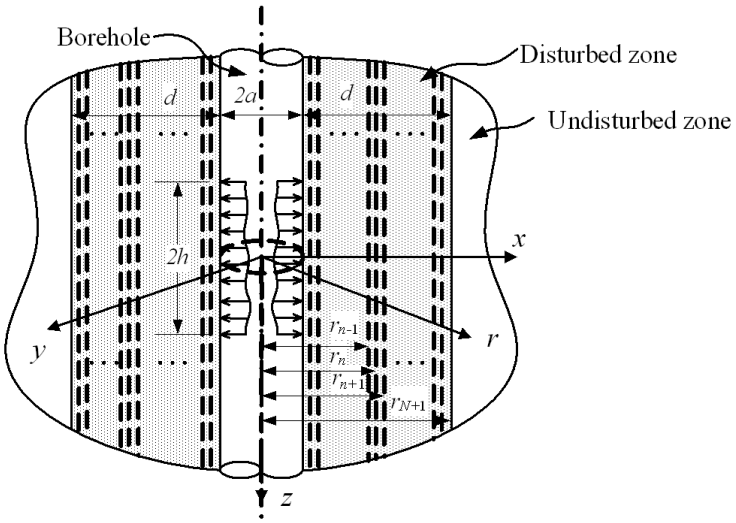

Figure 1: Infinite borehole in poroelastic medium with excavation disturbed zone.

$$\sigma_{rz} = \mu \left(\frac{\partial u_r}{\partial z} + \frac{\partial u_z}{\partial r} \right) \tag{8}$$

where σ_{rr}, $\sigma_{\theta\theta}$, σ_{zz} and σ_{rz} denote the total stress components of the bulk material, and p is the excess pore fluid pressure (suction is considered negative), which can be expressed in terms of dilatation and variation of fluid volume as

$$p = -\alpha M\varepsilon + M\zeta \tag{9}$$

In addition, the fluid discharge in the i-direction ($i = r,z$), denoted by q_i, is defined as

$$q_i = \frac{\partial w_i}{\partial t} \tag{10}$$

The governing equations, Eqs. (1)-(4), can be solved by using the following Helmholtz representation for axisymmetric vector fields.

$$u_r(r,z,t) = \frac{\partial \phi_1}{\partial r} + \frac{\partial^2 \varphi_1}{\partial r \partial z} \tag{11}$$

$$u_z(r,z,t) = \frac{\partial \phi_1}{\partial z} - \frac{1}{r}\frac{\partial}{r}\left(r\frac{\partial \varphi_1}{\partial r}\right) \tag{12}$$

$$w_r(r,z,t) = \frac{\partial \phi_2}{\partial r} + \frac{\partial^2 \varphi_2}{\partial r \partial z} \tag{13}$$

$$w_z(r,z,t) = \frac{\partial \phi_2}{\partial z} - \frac{1}{r}\frac{\partial}{r}\left(r\frac{\partial \varphi_2}{\partial r}\right) \tag{14}$$

where ϕ_i(i=1, 2) and φ_i(i=1,2) are scalar and vector fields respectively.

Substituting Eqs. (11)-(14) into Eqs. (1)-(4) together with the assumption that the motion is time-harmonic with a factor of $e^{i\omega t}$ where ω is the frequency of excitation, yields two sets of partial different equations for scalar fields φ_1, φ_2 and vector fields ϕ_1, ϕ_2 as follows:

$$\left[(\lambda + \alpha M + 2\mu)\nabla^2 + \rho\omega^2\right]\varphi_1 = -\left(\alpha M\nabla^2 + \rho_f\omega^2\right)\varphi_2 \tag{15}$$

$$\left(\alpha M\nabla^2 + \rho_f\omega^2\right)\varphi_1 = -\left(M\nabla^2 + m\omega^2 - ib\omega\right)\varphi_2 \tag{16}$$

and

$$\left(\mu\nabla^2 + \rho\omega^2\right)\phi_1 = -\omega^2\rho_f\phi_2 \tag{17}$$

$$\omega^2\rho_f\phi_1 = -\omega^2 m\phi_2 + i\omega b\phi_2 \tag{18}$$

Note that the term $e^{i\omega t}$ is suppressed from all expressions for brevity. The above partial differential equations are reduced to ordinary differential equations by performing Fourier transform with respect to the z-coordinate. The Fourier transform

of a function $f(r,z)$ with respect to the vertical coordinate and the inverse relationship are given by [Sneddon (1951)]

$$\tilde{f}(r,\xi) = \frac{1}{2\pi}\int_{-\infty}^{\infty} f(r,z)e^{i\xi z}dz \tag{19}$$

$$f(r,z) = \int_{-\infty}^{\infty} \tilde{f}(r,\xi)e^{-i\xi z}d\xi \tag{20}$$

where a tilde ($\tilde{}$) denotes the Fourier transform of a function and ξ is the Fourier transform parameter.

After lengthy manipulations, it can be shown that the general solutions of Fourier transforms of φ_i(i=1, 2) and ϕ_i(i=1,2) can be expressed as

$$\tilde{\varphi}_1(r,\xi) = AI_0(\gamma_1 r) + BK_0(\gamma_1 r) + CI_0(\gamma_2 r) + DK_0(\gamma_2 r) \tag{21}$$

$$\tilde{\varphi}_2(r,\xi) = \chi_1\left[AI_0(\gamma_1 r) + BK_0(\gamma_1 r)\right] + \chi_2\left[CI_0(\gamma_2 r) + DK_0(\gamma_2 r)\right] \tag{22}$$

$$\tilde{\phi}_1(r,\xi) = EI_0(\gamma_3 r) + FK_0(\gamma_3 r) \tag{23}$$

$$\tilde{\phi}_2(r,\xi) = \chi_3\left[EI_0(\gamma_3 r) + FK_0(\gamma_3 r)\right] \tag{24}$$

where $A(\xi)$, $B(\xi)$, $C(\xi)$, $D(\xi)$, $E(\xi)$, and $F(\xi)$ are arbitrary functions to be determined by applying appropriate boundary and/or continuity conditions relevant to a given problem, and γ_i (i=1, 2, 3) and χ_i (i=1, 2, 3) are defined in Appendix A. In addition, I_n and K_n are modified Bessel functions of the first and second kinds respectively of order n [Watson (1944)]. Thereafter, the general solutions for displacements, stresses, excess pore pressure and fluid discharge can be obtained in terms of the arbitrary functions, $A(\xi)$ to $F(\xi)$, by using Eqs. (5)-(14), as follows:

$$\begin{aligned}\tilde{u}_r =& \gamma_1\left[AI_1(\gamma_1 r) - BK_1(\gamma_1 r)\right] + \gamma_2\left[CI_1(\gamma_2 r) - DK_1(\gamma_2 r)\right] \\ &+ i\xi\gamma_3\left[EI_1(\gamma_3 r) - FK_1(\gamma_3 r)\right]\end{aligned} \tag{25}$$

$$\tilde{u}_z = i\xi\left[AI_0(\gamma_1 r) + BK_0(\gamma_1 r) + CI_0(\gamma_2 r) + DK_0(\gamma_2 r)\right] - \gamma_3^2\left[EI_0(\gamma_3 r) + FK_0(\gamma_3 r)\right] \tag{26}$$

$$\begin{aligned}\tilde{w}_r =& \gamma_1\chi_1\left[AI_1(\gamma_1 r) - BK_1(\gamma_1 r)\right] + \gamma_2\chi_2\left[CI_1(\gamma_2 r) - DK_1(\gamma_2 r)\right] \\ &+ i\xi\gamma_3\chi_3\left[EI_1(\gamma_3 r) - FK_1(\gamma_3 r)\right]\end{aligned} \tag{27}$$

$$\begin{aligned}\tilde{w}_z =& i\xi\left\{\chi_1\left[AI_0(\gamma_1 r) + BK_0(\gamma_1 r)\right] + \chi_2\left[CI_0(\gamma_2 r) + DK_0(\gamma_2 r)\right]\right\} \\ &- \gamma_3^2\chi_3\left[EI_0(\gamma_3 r) + FK_0(\gamma_3 r)\right]\end{aligned} \tag{28}$$

$$\tilde{p} = \eta_1 [AI_0(\gamma_1 r) + BK_0(\gamma_1 r)] + \eta_2 [CI_0(\gamma_2 r) + DK_0(\gamma_2 r)] \tag{29}$$

$$\begin{aligned}\tilde{\sigma}_{rr} =& \beta_1 [AI_0(\gamma_1 r) + BK_0(\gamma_1 r)] - 2\mu\gamma_1 r^{-1} [AI_1(\gamma_1 r) - BK_1(\gamma_1 r)] \\ &+ \beta_2 [CI_0(\gamma_1 r) + DK_0(\gamma_1 r)] - 2\mu\gamma_2 r^{-1} [CI_1(\gamma_1 r) - DK_1(\gamma_1 r)] \\ &+ i\xi\gamma_3^2 [EI_0(\gamma_3 r) + FK_0(\gamma_3 r)] - i\xi\gamma_3 r^{-1} [EI_1(\gamma_3 r) - FK_1(\gamma_3 r)]\end{aligned} \tag{30}$$

$$\begin{aligned}\tilde{\sigma}_{\theta\theta} =& -(\lambda L_1^2 + \alpha\eta_1) [AI_0(\gamma_1 r) + BK_0(\gamma_1 r)] + 2\mu\gamma_1 r^{-1} [AI_1(\gamma_1 r) - BK_1(\gamma_1 r)] \\ &- (\lambda L_2^2 + \alpha\eta_2) [CI_0(\gamma_2 r) + DK_0(\gamma_2 r)] + 2\mu\gamma_2 r^{-1} [CI_1(\gamma_2 r) - DK_1(\gamma_2 r)] \\ &+ 2\mu i\xi\gamma_3 r^{-1} [EI_1(\gamma_3 r) - FK_1(\gamma_3 r)]\end{aligned} \tag{31}$$

$$\begin{aligned}\tilde{\sigma}_{zz} =& -(2\mu\xi^2 + \lambda L_1^2 + \alpha\eta_1) [AI_0(\gamma_1 r) + BK_0(\gamma_1 r)] \\ &- (2\mu\xi^2 + \lambda L_2^2 + \alpha\eta_2) [CI_0(\gamma_1 r) + DK_0(\gamma_1 r)] \\ &- 2\mu i\xi\gamma_3^2 [EI_0(\gamma_3 r) + FK_0(\gamma_3 r)]\end{aligned} \tag{32}$$

$$\begin{aligned}\tilde{\sigma}_{rz} =& 2\mu i\xi\gamma_1 [AI_1(\gamma_1 r) - BK_1(\gamma_1 r)] + 2\mu i\xi\gamma_2 [CI_1(\gamma_1 r) - DK_1(\gamma_1 r)] \\ &- \mu\gamma_3(\xi^2 + \gamma_3^2) [EI_1(\gamma_3 r) - FK_1(\gamma_3 r)]\end{aligned} \tag{33}$$

where η_i, β_i, and L_i(i=1, 2) are defined in Appendix A.

It can be shown that the general solutions for axisymmetric deformations of a poroelastic medium in the Fourier transform domain, given by Eqs. (25)-(33), can be expressed in the following matrix form.

$$\mathbf{u}(r,\xi) = \mathbf{R}(r,\xi)\mathbf{C}(\xi) \tag{34}$$

$$\mathbf{f}(r,\xi) = \mathbf{S}(r,\xi)\mathbf{C}(\xi) \tag{35}$$

where

$$\mathbf{u}(r,\xi) = \begin{bmatrix} \tilde{u}_r & \tilde{u}_z & \tilde{p} \end{bmatrix}^T \tag{36}$$

$$\mathbf{f}(r,\xi) = \begin{bmatrix} \tilde{\sigma}_{rr} & \tilde{\sigma}_{rz} & \tilde{w}_r \end{bmatrix}^T \tag{37}$$

and

$$\mathbf{C}(\xi) = \begin{bmatrix} A & B & C & D & E & F \end{bmatrix}^T \tag{38}$$

The elements of matrices **R** and **S** in the above equations are given in Appendix A. In the ensuing section, the general solutions are employed to establish an exact stiffness matrix scheme to investigate dynamic response of a borehole in a poroelastic medium with excavation disturbed zone.

3 Borehole in excavation disturbed zone

Naturally, a primary factor affecting the soil/rock properties around a borehole is an excavation process. The zone where the properties and conditions have been changed is known as an excavation disturbed zone (EDZ) [Sato, Kikuchi and Sugihara (2000); Martio and Chandler (2004); Malmgren, Saiang, Töyrä and Bodare (2007); Shao, Schuster, Sonnke and Brauer (2008); Kwon and Cho (2008); Kwon, Lee, Cho, Jeon and Cho (2009)]. The properties of the EDZ could be estimated based on laboratory and in situ tests [Lai, Cai, Ren, Xie and Esaki (2006); Kwon, Lee, Cho, Jeon and Cho (2009)]. The shear modulus of the EDZ is normally reduced from its original value before excavation. On the other hand, the permeability in the EDZ could be increased from the original value due to an excavation. Consider a cylindrical borehole with the EDZ of a length d as shown in Fig. 1. It is assumed that the shear modulus in the EDZ linearly decreases from the borehole surface, and the permeability in the medium increases uniformly in the disturbed zone according to the following equations.

$$\mu(r) = \mu_0 [m_1(r-a-d)+1] \tag{39}$$

and

$$b(r) = m_2 b_0 \tag{40}$$

where μ_0 and b_0 denote the original values of the shear modulus and the parameter b, which is defined as a ratio between fluid viscosity and intrinsic permeability, respectively before excavation. In addition, m_1 and m_2 are non-negative constants representing the degree of disturbance due to drilling process in the shear modulus and the parameter b respectively. Since b is inversely proportional to permeability, m_2 should then be less than one. The poroelastic medium in Fig. 1 is then separated into two zones, i.e. the disturbed zone ($a \leq r < d$) and the undisturbed zone ($r > d$). To incorporate the influence of excavation disturbed zone, the EDZ is discretized into a total of N infinitely long tubular layers with small thickness perfectly bonded together. Each discretized layer is homogeneous and governed by Biot's poroelastodynamics theory. The following relationship can be established by using Eqs. (34) and (35) for the n^{th} layer.

$$\mathbf{F}^{(n)} = \mathbf{K}^{(n)} \mathbf{U}^{(n)} \tag{41}$$

where $\mathbf{K}^{(n)}$ is an exact stiffness matrix in the Fourier transform space describing the relationship between the generalized displacement vector $\mathbf{U}^{(n)}$ and the generalized force vector $\mathbf{F}^{(n)}$ for the n^{th} layer, in which,

$$\mathbf{U}^{(n)} = \left[\begin{array}{cc} \mathbf{u}^{(n)}(r_n, \xi) & \mathbf{u}^{(n)}(r_{n+1}, \xi) \end{array} \right]^T \tag{42}$$

$$\mathbf{F}^{(n)} = \left[\begin{array}{cc} -\mathbf{f}^{(n)}(r_n,\xi) & \mathbf{f}^{(n)}(r_{n+1},\xi) \end{array} \right]^T \tag{43}$$

In Eqs. (42) and (43), $\mathbf{U}^{(n)}$ is a column vector of generalized displacements of the n^{th} layer whose elements are related to the Fourier transforms of displacements and pore pressure of the inner ($r = r_n$) and outer ($r = r_{n+1}$) surfaces of the n^{th}layer; $\mathbf{F}^{(n)}$ is a column vector of generalized forces whose elements are related to the Fourier transforms of traction and fluid displacement of the inner and outer surfaces of the n^{th} layer. In addition, the matrices $\mathbf{u}^{(n)}$ and $\mathbf{f}^{(n)}$ are identical to $\mathbf{u}$ and $\mathbf{f}$ given by Eqs. (34) and (35) respectively, except that the material properties of the n^{th} layer are employed with $r = r_n$ or $r = r_{n+1}$. Similarly, the stiffness matrix $\mathbf{K}^{(N+1)}$ for the undisturbed zone ($r > d$ in Fig. 1) is obtained by establishing the relationship between the generalized displacement vector $\mathbf{U}^{(N+1)}$ and the generalized force vector $\mathbf{F}^{(N+1)}$.

The global stiffness matrix of the EDZ can be assembled by using the continuity conditions of traction and fluid flow at the layer interfaces. The final equation system can be expressed as

$$\mathbf{F}^* = \mathbf{K}^* \mathbf{U}^* \tag{44}$$

where $\mathbf{K}^*$ is a global stiffness matrix, which is a symmetric matrix with a bandwidth of 6. In addition, $\mathbf{U}^*$ and $\mathbf{F}^*$ are the global vectors of generalized displacements and generalized forces defined as

$$\mathbf{U}^* = \left[\begin{array}{ccccccc} \mathbf{u}^{(1)} & \mathbf{u}^{(2)} & \cdots & \mathbf{u}^{(n)} & \cdots & \mathbf{u}^{(N)} & \mathbf{u}^{(N+1)} \end{array} \right]^T \tag{45}$$

$$\mathbf{F}^* = \left[\begin{array}{ccccccc} \mathbf{f}^{(1)} & \mathbf{f}^{(2)} & \cdots & \mathbf{f}^{(n)} & \cdots & \mathbf{f}^{(N)} & \mathbf{f}^{(N+1)} \end{array} \right]^T \tag{46}$$

Consider a borehole in a poroelastic medium with the EDZ subjected to axisymmetric loading as shown in Fig. 1. The boundary conditions for a borehole under applied radial traction $F_r(z)$ and applied vertical traction $F_z(z)$ are given by

$$\tilde{\sigma}_{rr}(1,\xi) = \tilde{F}_r(\xi) \tag{47}$$

$$\tilde{\sigma}_{rz}(1,\xi) = \tilde{F}_z(\xi) \tag{48}$$

$$\text{and} \quad \tilde{p}(1,\xi) = 0 \quad \text{for fully permeable surface} \tag{49}$$

$$\text{or} \quad \tilde{q}_r(1,\xi) = 0 \quad \text{for impermeable surface} \tag{50}$$

The boundary conditions for a borehole under applied fluid pressure $P(z)$ are given by

$$\tilde{\sigma}_{rr}(1,\xi) = -\alpha \tilde{P}(\xi) \tag{51}$$

$$\tilde{\sigma}_{rz}(1,\xi) = 0 \tag{52}$$

and

$$\tilde{p}(1,\xi) = \tilde{P}(\xi) \tag{53}$$

The boundary conditions for a borehole under applied fluid discharge $Q(z)$ are given by

$$\tilde{\sigma}_{rr}(1,\xi) = -\alpha\tilde{p}(\xi) \tag{54}$$

$$\tilde{\sigma}_{rz}(1,\xi) = 0 \tag{55}$$

and

$$\tilde{q}_r(1,\xi) = \tilde{Q}(\xi) \tag{56}$$

4 Numerical results and discussion

A computer program has been developed based on the solution procedure described in the previous section to solve boundary value problems related to a borehole in a poroelastic medium with excavation disturbed zone under axisymmetric time-harmonic loading. This requires the solution of the system of linear simultaneous equations given by Eq. (44). Since Eq. (44) is established in the Fourier transform space, it has to be solved for discrete values of ξ. The integral with respect to ξ can be reduced to a semi-infinite integral since the integrand is either an even or odd function of ξ. To evaluate such integral numerically, it is common to truncate the domain of integration from (0,∞) to (0, ξ_L) where ξ_L is a finite real number. This integral is then computed by using an adaptive numerical quadrature scheme that subdivides the interval of integration. The integral over each subinterval is evaluated by employing a 21-point Gauss–Kronrod rule. The subdivision continues until the error from the approximation is less than a specified tolerance. A convergence study was carried out to determine appropriate values of ξ_L used in the truncation of the semi-infinite integrals, and the number of tubular layers (N) used in the discretization of the EDZ. It is found that converged numerical results are obtained when $\xi_L \geq 100$ and $N \geq 20$. All numerical results presented in this paper thus correspond to the cases where ξ_L=100 and N=20.

4.1 Comparison with existing solutions

The accuracy of the present solution scheme is verified by comparing with the existing dynamic solutions for a borehole in both elastic and poroelastic media without a disturbed zone. Parnes (1986) presented time-harmonic response of a cylindrical

borehole in an elastic medium due to axisymmetric traction applied at its surface. Fig. 2(a) shows comparisons of nondimensional radial displacement and tangential stress along the radial direction (z/a=0) due to a radial ring load of magnitude P. Poisson's ratio equal to 0.25 and a nondimensional frequency of δ=2.0, defined as $\delta = \omega a\sqrt{\rho/\mu_0}$, are used. The present solution is obtained by using 20 tubular layers ($N = 20$) of identical properties. In addition, $m_1 = 0$ and $m_2 = 1$ are considered to represent a borehole without the disturbed zone. Excellent agreement between the two solutions is noted in Fig. 2(a). Fig. 2(b) shows comparisons of vertical variations of the amplitudes of radial displacement and vertical stress at r/a=1.5 due to a radial ring load of magnitude P applied at z/a= 0 of a borehole in a poroelastic medium without the disturbed zone between the present solutions and those given by Lu and Jeng (2006). The following material parameters are used: λ/μ_0=0.333; M/μ_0=0.667; ρ_f/ρ=0.488; α=0.95; m/ρ=3.333; and $b^* = ab_0/\sqrt{\rho\mu_0}$= 577.40. The borehole diameter is equal to $2a$, and its surface is assumed to be fully permeable. Two nondimensional frequencies of δ=5.73 and 11.45 are considered. Excellent agreement is once again observed between the present solutions and the solutions given by Lu and Jeng (2006). The accuracy of the present solution scheme is thus confirmed through these independent comparisons.

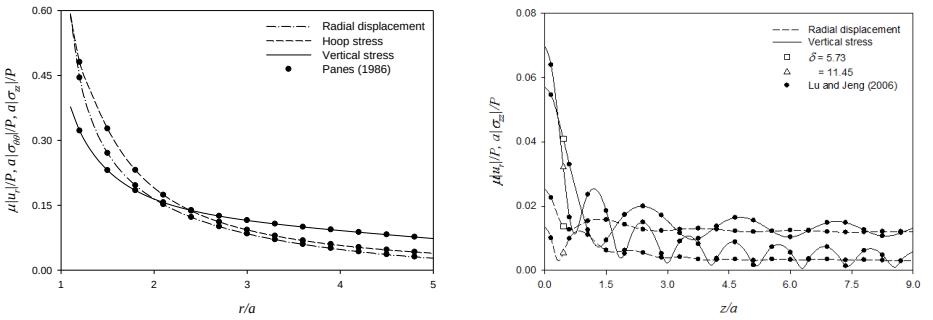

(a) (b)

Figure 2: Comparison with existing solutions for a borehole in (a) elastic medium and (b) poroelastic medium.

4.2 Borehole under applied radial traction

The first set of numerical results corresponds to the case where axisymmetric radial traction of magnitude f_0 is applied over a finite segment of h/a=1 at the borehole surface (see Fig. 1). The following nondimensional parameters are considered for the surrounding poroelastic medium in all numerical results presented hereafter: λ/μ_0=0.333; M/μ_0=0.667; ρ_f/ρ=0.5; α=0.95 and m/ρ=3.333. The influence

from the size of excavation disturbed zone is presented first. Fig. 3 presents radial profiles of non-dimensional radial displacement at the mid-plane ($z/a = 0$) of a fully permeable wall with b^*=1. The lengths of the excavation disturbed zone, varied from $d/a = 1$ to 5, with m_1=0.1 and m_2=0.001 are considered. The influence from the size of EDZ on the radial displacement in the vicinity of the borehole wall ($r/a < 3$) is clearly observed from the results presented in Fig. 3.

Nondimensional radial displacement at the center of loading ($r/a = 1$, $z/a = 0$) are presented in Fig. 4 for the frequency range $0 < \delta \leq 10$. The shear modulus is assumed to be linearly varied with the radial direction (m_1 = 0, 0.1 and 0.2) whereas the permeability in the medium is assumed to be unchanged from the excavation, i.e. m_2=1.0. Two extreme cases of the hydraulic boundary conditions at the borehole surface, i.e. fully permeable and impermeable, are considered. In addition, the size of disturbed zone considered in this figure and in all figures presented hereafter is assumed to be twice the borehole diameter, i.e. $d/a = 4$ [Sato, Kikuchi and Sugihara (2000)]. Numerical results in Fig. 4 indicate that the change in shear modulus in the excavation disturbed zone has a significant influence on the radial displacement. Radial variations of both real and imaginary parts with δ for the same value of m_1 are similar for fully permeable and impermeable borehole walls. Both real and imaginary parts of the radial displacement show more oscillatory variation with δ for the borehole with higher degree of change in shear modulus (higher value of m_1). In addition, the radial displacement also increases with increasing m_1 when $\delta < 2$. The influence of internal friction between solid and fluid, represented by the parameter b, on the radial displacement is also considered with b^*=1 and 1000 in Fig. 4. It is found that the difference between the solutions with b^*= 1 and 1000 is typically within 5% for both real and imaginary parts irrespective of the hydraulic boundary condition at the borehole wall.

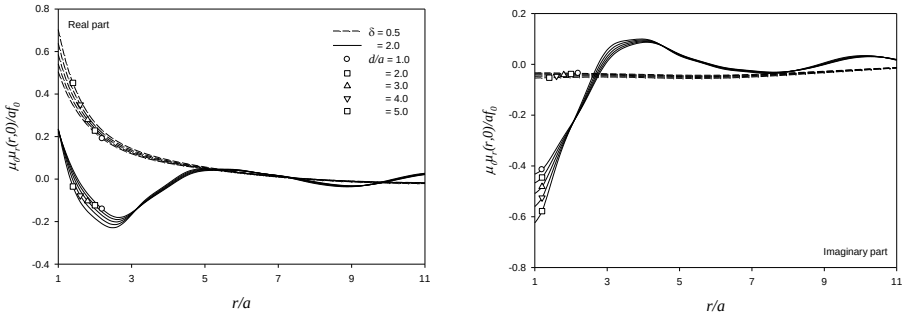

Figure 3: Profiles of radial displacement along the r-axis due to applied radial traction at permeable wall.

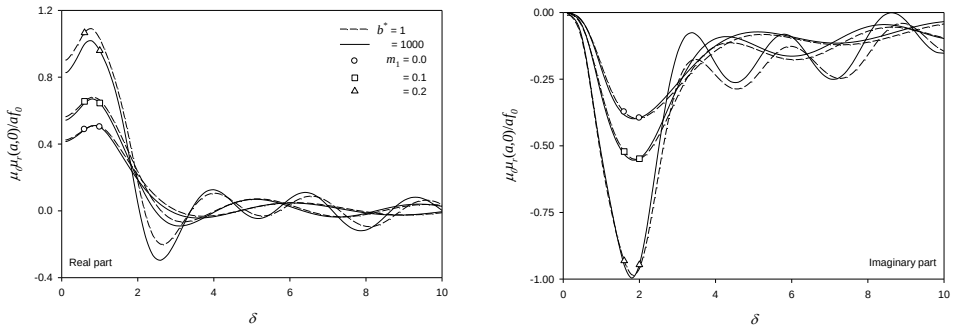

(a)

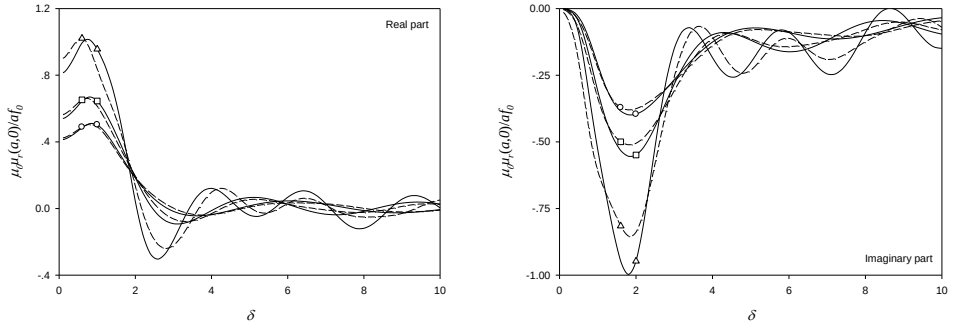

(b)

Figure 4: Radial displacement at the center of loading due to radial traction on (a) permeable wall and (b) impermeable wall.

Nondimensional tangential stresses at the center of loading (r/a = 1, z/a = 0) are presented for both fully permeable and impermeable borehole walls in Figs. 5(a) and 5(b) respectively. Tangential stress around the borehole is useful in the study of borehole stability and fracturing. For a fully permeable borehole wall, both real and imaginary parts of tangential stress show minor dependence on the internal friction between solid and fluid (parameter b) similar to what observed from the radial displacement presented in Fig. 4, whereas the internal friction has more influence on the impermeable borehole. Contrarily to the radial displacement results shown in Fig. 4, tangential stress decreases with increasing m_1 when $\delta < 2$. At higher frequencies ($\delta \geq 2$), both real and imaginary parts of tangential stress show more complicated variations with m_1.

Nondimensional excess pore pressure at the center of loading ($r/a = 1$ and z/a= 0) due to radial traction applied at an impermeable borehole wall is presented in Fig.

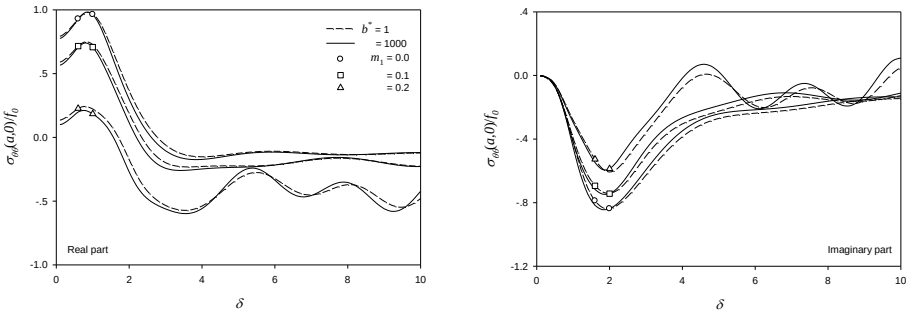

(a)

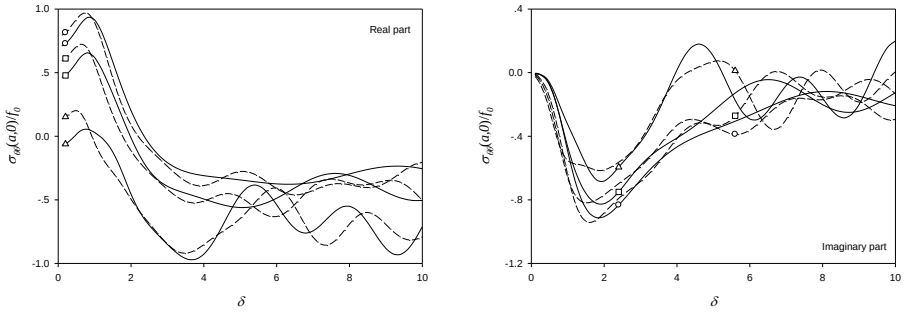

(b)

Figure 5: Tangential stress at the center of loading due to radial traction on (a) permeable wall and (b) impermeable wall.

6(a). Numerical results presented in Fig. 6(a) indicate that excess pore pressure depends very significantly on the internal friction b^* and the change in shear modulus m_1. It can be seen that excess pore pressure corresponding to b^*=1 shows more oscillatory variation with δ when compared to that of b^*=1000. Excess pore pressure increases with increasing m_1 at lower frequencies ($\delta < 4$) whereas it shows complicated variations with higher frequencies ($\delta > 4$). Figure 6(b) presents nondimensional radial fluid discharge at the center of loading due to applied radial traction at a fully permeable borehole wall. As expected, both real and imaginary parts of fluid discharge are negligible when$\delta \to 0$. It is also found that radial discharge corresponding to b^*=1 is larger than that of b^*=1000 since b^* is inversely proportional to permeability, and it shows more oscillatory variation withδ similar to what observed from the excess pore pressure shown in Fig. 6(a). In addition, both real and imaginary parts of the radial discharge show minor dependence on the effect

of EDZ when b^*=1000 over the whole frequency range of $\delta < 10$.

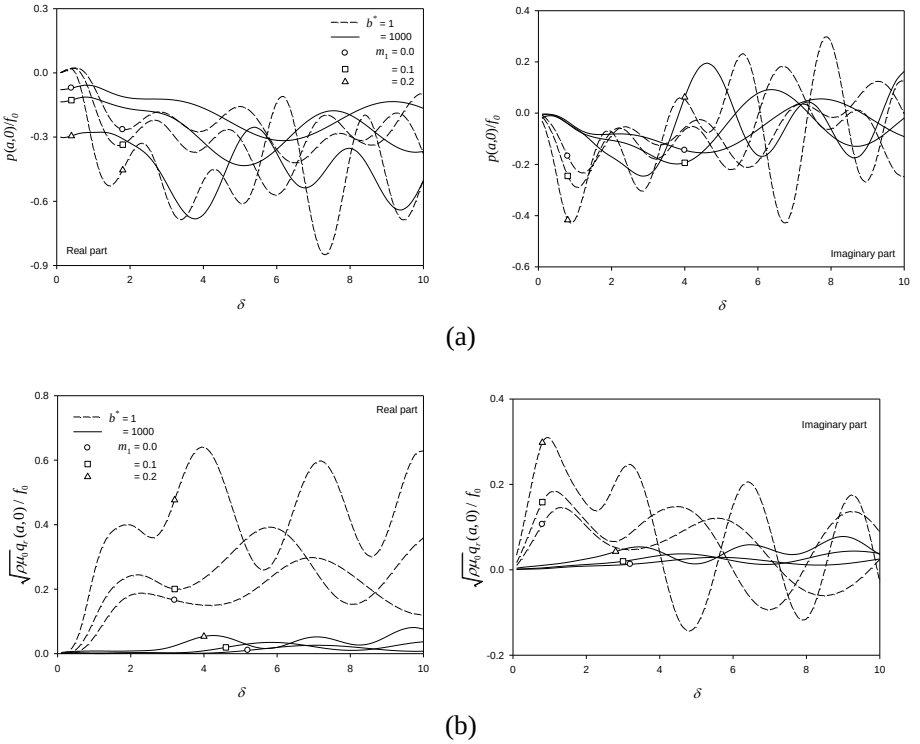

Figure 6: (a) Excess pore pressure and (b) radial discharge at the center of loading due to applied radial traction.

Next, radial variations of nondimensional radial displacement, tangential stress, excess pore pressure, and fluid discharge due to uniform radial traction are illustrated in Figs. 7 and 8 along the plane z/a=0. Solutions are presented for b^*=1 with m_1=0, 0.1 and 0.2, and δ= 0.5 and 2.0. It can be seen from figure 7 that both radial displacement and tangential stress in the vicinity of borehole ($r/a < 3$) depend significantly on both δ and m_1. The maximum values of both real and imaginary parts of radial displacement for $\delta = 0.5$ occur at the borehole wall before decaying with the radial distance. For higher frequency (δ=2.0), the displacement profiles show more oscillatory variations, but the maximum values are still found at the borehole wall. The radial displacement decreases with increasing the value of m_1 in the vicinity of borehole ($r/a < 3$), and the influence from the EDZ on the displacement could be neglected when $r/a > 5$. Radial profiles of nondimensional tangential stress in Fig. 7(b) reveal that the maximum stresses are observed at the borehole wall, and then

decay along the radial distance. The tangential stress deceases with increasing m_1. In addition, the profiles of tangential stress for δ=2 show more oscillatory variation than those of the radial displacement shown in Fig. 7(a).

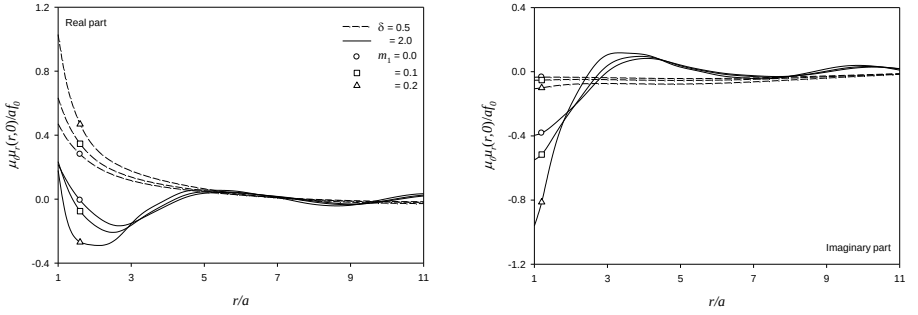

(a)

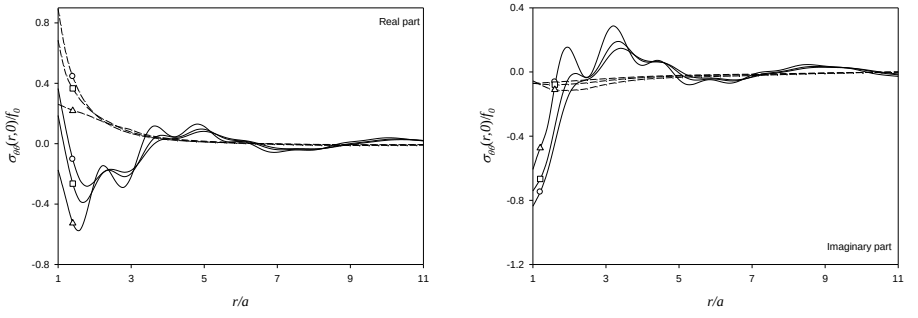

(b)

Figure 7: Profiles of (a) radial displacement and (b) tangential stress along the r-axis due to applied radial traction at permeable wall.

Figs. 8(a) and 8(b) present variations of nondimensional excess pore pressure and fluid discharge respectively along the radial direction at the mid-plane (z/a=0) for fully permeable borehole surface. Numerical results indicate that the excavation disturbed zone has a significant influence on both excess pore pressure and fluid discharge for $\delta = 2.0$, whereas the solutions at lower frequency (δ=0.5) are nearly independent of m_1, especially when $r/a > 5$. Both real and imaginary parts of pore pressure when $\delta = 2.0$ show oscillatory variation along the radial direction. The peak values of fluid discharge shown in Fig. 8(b) are observed at the borehole surface, which are the same as those of the radial displacement and tangential stress presented in Fig. 7. This is consistent with the fact that the maximum solutions

occur at the point of applied loading. Excess pore pressure is equal to zero at the wall due to the specified boundary condition. In addition, both excess pore pressure and fluid discharge diminish to negligible level when $r/a > 10$.

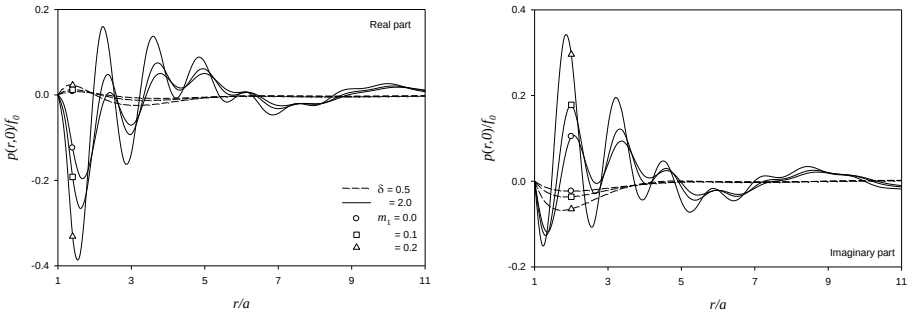

(a)

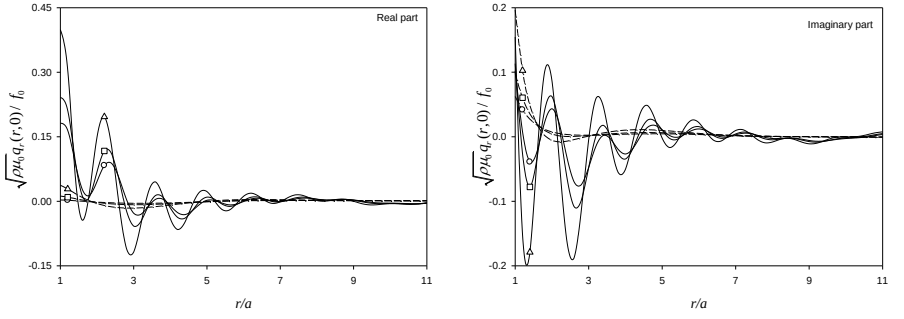

(b)

Figure 8: Profiles of (a) excess pore pressure and (b) radial discharge along the r-axis due to applied radial traction at a permeable wall.

4.3 Borehole under applied fluid pressure

The final set of numerical results corresponds to the case where time-harmonic fluid pressure of magnitude p_0 is applied over segment of h/a=1 at the borehole wall (see Fig. 1). The permeability in the disturbed zone is changed according to Eq. (40) with m_2 = 0.1, 0.5 and 1.0 whereas the shear modulus in the medium remains the same, i.e. m_1 = 0. In addition, the solutions in Figs. 9 and 10 are presented for b^*= 1. Figs. 9(a) and 9(b) show radial variations of nondimensional radial displacement and tangential stress respectively along the mid-plane (z/a= 0) over the range $0 \leq r/a \leq 5$. Radial profiles presented in Figure 9 reveal that

radial displacement and tangential stress show minor dependence on the change in permeability (m_2). It can also be seen that radial profiles of radial displacement and tangential stress for $\delta = 0.5$ are quite smooth along the plane $z/a = 0$ when compared to oscillatory variations observed in the displacement and stress profiles for $\delta = 2.0$. It is noted that the displacement and tangential stress due to the applied fluid pressure can be neglected when $r/a > 5$.

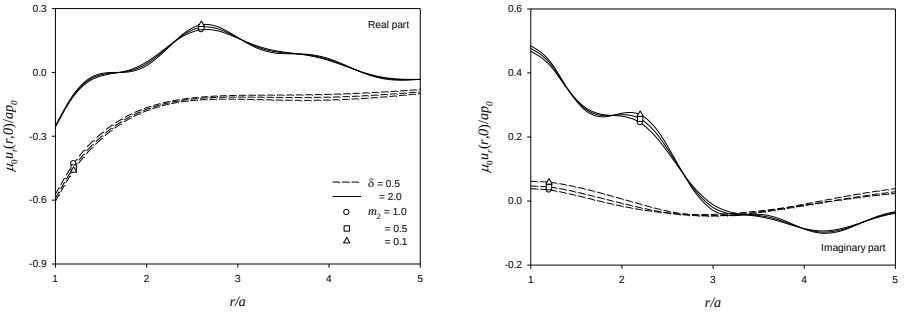

(a)

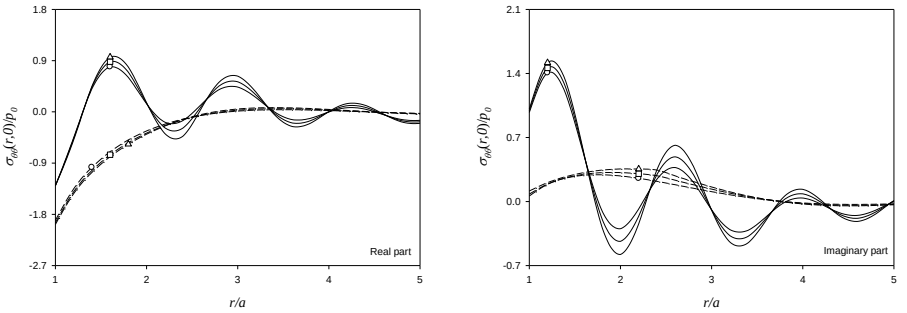

(b)

Figure 9: Profiles of (a) radial displacement and (b) tangential stress along the r-axis due to applied fluid pressure.

Figures 10(a) and 10(b) present profiles of nondimensional excess pore pressure and fluid discharge respectively along the radial distance $0 \leq r/a \leq 5$ at $z/a = 0$ due to time-harmonic fluid pressure applied at the borehole surface. It is found that both real and imaginary parts of both pore pressure and fluid discharge show smooth variations with r/a for $\delta = 0.5$, but more oscillatory variations when $\delta = 2.0$ similar to what observed from radial displacement and tangential stress profiles illustrated in Fig. 9. At $\delta = 0.5$, both pore pressure and fluid discharge are maximal at

the borehole surface and decrease along the radial distance before diminish to negligible level when $r/a > 5$. At higher frequency ($\delta = 2.0$), both pore pressure and discharge show more dependence on the change in permeability in the excavation disturbed zone. It is found that a borehole with higher value of m_2 shows lower amplitudes of pore pressure and discharge than those correspond to lower value of m_2.

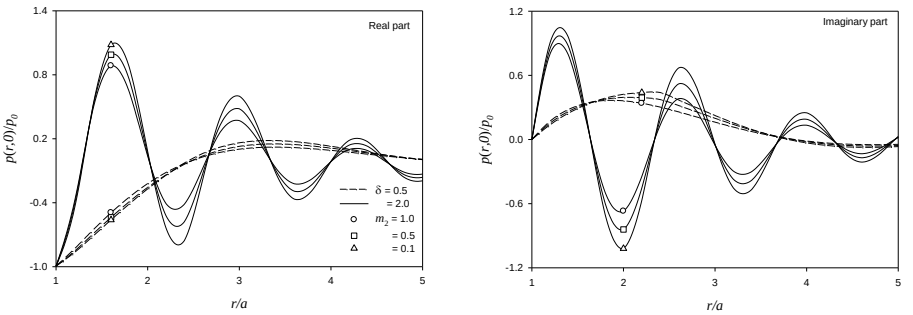

(a)

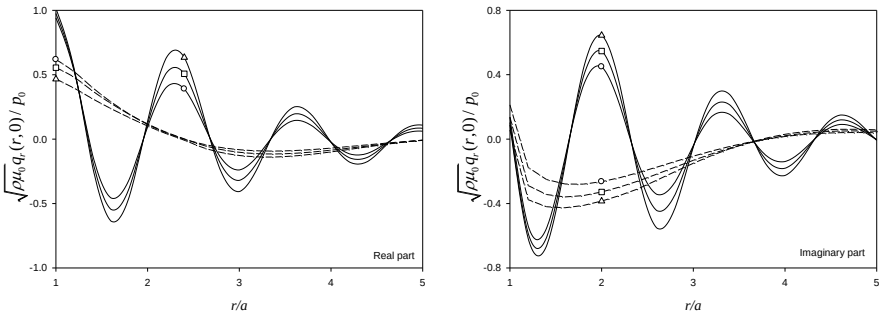

(b)

Figure 10: Profiles of (a) excess pore pressure and (b) radial discharge due to applied fluid pressure.

5 Conclusion

The dynamic response of a cylindrical borehole in a poroelastic medium with an excavation disturbed zone subjected to time-harmonic loading is presented in this paper. A set of general solutions to the governing equations from Biot's poroelastodynamics theory is derived by using Helmholtz representation for axisymmetric

vector fields and the Fourier integral transforms. These solutions are used to formulate boundary value problems corresponding to a borehole with the disturbed zone subjected to axisymmetric loading applied at its surface. The presented numerical results indicate that dynamic response of borehole depends on several factors such as material properties, degree of disturbance from drilling process, hydraulic boundary conditions along the borehole surface and the loading types. It is found that radial displacement, tangential stress, pore pressure and fluid discharge depend significantly on the change in shear modulus in the disturbed zone. The influence of internal friction due to relative motion between solid and fluid becomes less influence on radial displacement and tangential stress, but it has a significant influence on excess pore pressure and fluid discharge. The solutions along the radial direction show more oscillatory variations when the frequency excitation and the change in shear modulus increase. The solutions presented in this paper are useful to study several problems related to dynamic response of borehole in a poroelastic medium. For example, the present solutions can be employed to study wave propagation problems corresponding to the empty and liquid-filled cylindrical boreholes in a fluid-saturated porous medium. In addition, the derived analytical solutions can also be extended for stress analysis of a borehole under transient loadings by employing an appropriate technique such as the fast Fourier transforms.

References

Abousleiman, Y.; Chen, S. (2010): Poromechanics response of an inclined borehole subject to in-situ stress and finite length fluid discharge. *J Mech Mater Struct*, vol. 5, pp. 47–66.

Armand, G.; Lebon, P.; Cruchaudet, M.; Rebours, H.; Morel, J. and Wileveau, Y. (2007): Characterization of the excavation-damaged zone in the Meuse/Haute-Marne Underground Research Laboratory. *Proceeding in the 3rd International Meeting on Clays in Natural & Engineered Barriers for Radioactive Waste Confinement*.

Biot, M. A. (1941). General theory of three-dimensional consolidation. *J. Appl. Phys.,* vol. 12, pp. 155-164.

Biot, M. A. (1956). The theory of propagation of elastic waves in fluid-saturated porous solid. *J. Acous Aoc. Amer.*, vol. 28, pp. 168-191.

Biot, M. A. (1962). Mechanics of deformation and acoustic propagation in porous media. *J. Appl. Phys.*, vol. 33, pp. 1482–1498.

Cui, L.; Cheng, A. H-D. and Abousleiman, Y. (1997): Poroelastic solution for an inclined borehole. *J. Appl. Mech.* ASME, vol. 64, pp. 32-38.

Detournay E.; Cheng A. H-D. (1988): Poroelastic response of a borehole in non-

hydrostatic stress field. *Int J Rock Mech Min* vol. 25, pp. 171–82.

Jordan, D. W. (1962). The stress wave from a finite cylindrical explosive source. *J. Math. Mech.*, vol. 11, pp. 503-551.

Kaewjuea, W.; Senjuntichai, T. (2014): Poromechanical response of borehole in excavation disturbed zone. *Comput. Geotech.,* vol. 56, pp. 148-159.

Kwon, S.; Cho, W. J. (2008): The influence of an excavation damaged zone on the thermo-mechanical and hydro-mechanical behaviors of an underground excavation. *Eng. Geo.,* vol. 101, pp. 110-123.

Kwon, S.; Lee, C. S.; Cho, S. J.; Jeon, S. W.; Cho, W. J. (2009): An investigation of the excavation damaged zone at the KAERI underground research tunnel. *Tunn. Undergr. Sp. Tech.,* vol. 24, pp. 1-13.

Lai, X.; Cai, M.; Ren, F.; Xie, M.; Esaki, T. (2006): Assessment of rock mass characteristics and the excavation disturbed zone in the Lingxin Coal Mine beneath and Xitian river, China. *Int. J. Rock Mech. Min.,* vol. 43, pp. 572-581.

Lu J. F.; Jeng D. S. (2006): Dynamic analysis of a finite cylindrical hole in a saturated poroelastic medium. *Arch. Appl. Mech.*, vol. 76, pp. 263-276.

Malmgren, L.; Saiang, D.; Töyrä, J.; Bodare, A. (2007): The excavation disturbed zone (EDZ) at Kiirunavaara mine. *J. Appl. Geophys.*, vol. 61, pp. 1-15.

Martino, J. B.; Chandler, N. A. (2004): Excavation-induced damage studies at the Underground Research Laboratory. *Int. J. Rock Mech. Min.* vol. 41, pp. 1413-1426.

Parnes, R. (1986). Steady-state ring load pressure on a borehole surface. *Int. J. Solids Struct.*, vol. 22, pp. 73-86.

Rajapakse, R. K. N. D. (1993): Stress analysis of borehole in poroelastic medium. *J. Eng. Mech. ASCE*, vol. 119, pp. 1205–27.

Sato, T.; Kikuchi, T.; Sugihara K. (2000): In-situ experiments on an excavation disturbed zone induced by mechanical excavation in Neogene sedimentary rock at Tono mine, central Japan. *Eng. Geol.,* vol. 56, pp. 97-108.

Shao, H.; Schuster, K.; Sonnke, J.; Brauer, V. (2008): EDZ development in indurated clay formations-In situ borehole measurements and coupled HM modeling. *Phys. Chem. Earth.,* vol. 3, pp. S388-95.

Sneddon, I. N. (1951). *Fourier Transforms*. McGraw-Hill, New York.

Watson, G. N. (1962). *A treatise on the theory of Bessel functions*. 2^{nd} Ed., Cambridge University Press, Cambridge, England.

Appendix A

The matrices **R** and **S** in Eqs. (34) and (35) corresponding to dynamic response of a borehole problem are given by

$$\mathbf{R}=\begin{bmatrix} \gamma_1 I_1(\gamma_1 r) & -\gamma_1 K_1(\gamma_1 r) & \gamma_2 I_1(\gamma_2 r) & -\gamma_2 K_1(\gamma_2 r) & i\xi\gamma_3 I_1(\gamma_3 r) & -i\xi\gamma_3 K_1(\gamma_3 r) \\ i\xi I_0(\gamma_1 r) & i\xi K_0(\gamma_1 r) & i\xi I_0(\gamma_2 r) & i\xi K_0(\gamma_2 r) & -\gamma_3^2 I_0(\gamma_3 r) & -\gamma_3^2 K_0(\gamma_3 r) \\ \eta_1 I_0(\gamma_1 r) & \eta_1 K_0(\gamma_1 r) & \eta_2 I_0(\gamma_2 r) & \eta_2 K_0(\gamma_2 r) & 0 & 0 \end{bmatrix} \tag{A1}$$

$$\mathbf{S}=\begin{bmatrix} \beta_1 I_0(\gamma_1 r)-2\mu\gamma_1 r^{-1} I_1(\gamma_1 r) & \beta_1 K_0(\gamma_1 r)-2\mu\gamma_1 r^{-1} K_1(\gamma_1 r) & \beta_2 I_0(\gamma_2 r)-2\mu\gamma_2 r^{-1} I_1(\gamma_2 r) \\ 2\mu i\xi\gamma_1 I_1(\gamma_1 r) & -2\mu i\xi\gamma_1 K_1(\gamma_1 r) & 2\mu i\xi\gamma_2 I_1(\gamma_2 r) \\ \gamma_1\chi_1 I_1(\gamma_1 r) & -\gamma_1\chi_1 K_1(\gamma_1 r) & \gamma_2\chi_2 I_1(\gamma_2 r) \end{bmatrix}$$

$$\begin{bmatrix} \beta_2 K_0(\gamma_2 r)-2\mu\gamma_2 r^{-1} K_1(\gamma_2 r) & i\xi\gamma_3\left[\gamma_3 I_0(\gamma_3 r)-r^{-1} I_1(\gamma_3 r)\right] & i\xi\gamma_3\left[\gamma_3 K_0(\gamma_3 r)-r^{-1} K_1(\gamma_3 r)\right] \\ -2\mu i\xi\gamma_2 K_1(\gamma_1 r) & -\mu\gamma_3(\xi^2+\gamma_3^2) I_1(\gamma_3 r) & \mu\gamma_3(\xi^2+\gamma_3^2) K_1(\gamma_3 r) \\ -\gamma_2\chi_2 K_1(\gamma_2 r) & i\xi\gamma_3\chi_3 I_1(\gamma_3 r) & -i\xi\gamma_3\chi_3 K_1(\gamma_3 r) \end{bmatrix} \tag{A2}$$

where

$$\eta_i=(\alpha+\chi_i)ML_i^2,\ i=1,\ 2; \qquad \beta_i=2\mu\gamma_i^2-\lambda L_i^2-\alpha\eta_i,\ i=1,\ 2;$$

$$\chi_i=\frac{(\lambda+\alpha^2 M+2\mu)L_i^2-\rho\omega^2}{\rho_f\omega^2-\alpha ML_i^2},\ i=1,\ 2; \qquad \chi_3=\frac{\rho_f\omega^2}{ib\omega-m\omega^2}$$

$$\gamma_i=\sqrt{\xi^2-L_i^2},\ i=1,2 \qquad \gamma_3=\sqrt{\xi^2-S^2}$$

$$L_1^2=\frac{\varpi_1+\sqrt{\varpi_1^2-4\varpi_2}}{2} \qquad L_2^2=\frac{\varpi_1-\sqrt{\varpi_1^2-4\varpi_2}}{2}$$

$$S^2=\frac{(\rho_f\chi_3+\rho)\omega^2}{\mu}$$

$$\varpi_1=\frac{\left(m\omega^2-ib\omega\right)\left(\lambda+\alpha^2 M+2\mu\right)+\rho\omega^2 M-2\alpha\rho_f\omega^2 M}{(\lambda+2\mu)M}$$

$$\varpi_2=\frac{\left(m\omega^2-ib\omega\right)\rho\omega^2-\rho_f^2\omega^4}{M(\lambda+2\mu)}$$